Probing the underwater acoustic communication channel off Rottnest Island, Western Australia

Michael S. Caley[1] and Alec J. Duncan[1]

[1] Centre for Marine Science and Technology, Curtin University, Perth, Australia

ABSTRACT

The emerging field of underwater acoustic communication networks is under-pinned by accurate knowledge on the time-varying distortion of acoustic signals by the ocean. This paper reports on time-varying underwater acoustic channel responses measured over ranges of 100m to 10km in 50m deep water south-west of Rottnest Island, Western Australia, for 9-15kHz band signals. The channel response measurement techniques are described, including post-processing by correlative channel probing. The measured channel response spreading function is presented which conveys the spectrum of Doppler frequency shifts imparted by the ocean environment to transmitted data signals.

1. INTRODUCTION

1.1 What is a "channel"?

The term "channel" is used as an abbreviation of "communication channel". The communication channel is the physical medium that carries a signal between a transmitter and a receiver (Proakis, 2000), such as a wire, optical fibre, or the atmosphere. Here we mean the underwater environment between a transmitter and receiver.

Because signal transmission characteristics change depending on many physical and dimensional properties of the underwater environment, many distinctly different channels may be identified. So for example, transmission over a 100 m range in a given water depth is a distinctly different channel to transmission over a 1000 m range in the same water depth. The 100 m transmission range is a distinctly different channel on a day when the ocean surface is flat compared to a day when the surface is rough. Within a given environment, if the nature of the signal distortion and/or additive noise in two instances differ significantly, then the two channels are also distinct.

1.2 Shallow underwater acoustic channel challenges

Acoustic signal transmission through shallow underwater environments is subject to reverberant distortions from the superposition of delayed and scaled replica signal arrivals via multiple propagation paths. The relative timing of the multi-path arrival, known as delay-spreading, fluctuates due to time-varying elongation and contraction of transmission paths caused by surface-wave movement, which causes time-varying Doppler shifts in the signal frequency, or Doppler-spreading. In combination such channels are described as doubly-spread (Eggen et al., 2000)

The scale of time-varying Doppler has implications for the design of modern underwater acoustic signalling, such as Orthogonal Frequency Division Multiplexing (OFDM), where the transmission bandwidth of the modems (e.g. 9 kHz to 15 kHz) may be divided into as many as 512 narrow-frequency sub-carrier bands. Knowledge of the Doppler distortions in the channel informs how closely the signal sub-frequency bands may be spaced without causing inter-band signal interference.

The purpose of the underwater acoustic channel measurements described here was to assist the development of a time-varying underwater acoustic channel simulator (Caley, 2016). These measurements complement similar measurements reported previously in 13m water depth off Cottesloe Beach, Perth (Caley and Duncan, 2013). The simulator expands the scope for testing and development of underwater communications without the need for direct sea trials.

1.3 How a time-varying channel differs from a static channel

A static (time invariant) communication channel can be represented by an impulse response function $h(\tau)$ that describes the signal received at a time delay τ (s) after the transmission of an ideal impulse. A familiar example of a static acoustic channel is an auditorium considered between a stationary speaker and listener. The experience of multiple acoustic echoes after a clap within an acoustically reflective environment is an example of a time-invariant acoustic channel response that varies with delay since the clap instant.

A time-varying input signal $x(t)$ and a static channel response $h(\tau)$ combine to produce the time-varying channel output $y(t)$ at a receiver as per Eq.(1) (Proakis, 2000). The noise term $n(t)$ represents the received noise from the channel that is unrelated to the transmitted signal $x(t)$.

$$y(t) = \int_{-\infty}^{\infty} h(\tau)x(t-\tau)\, d\tau + n(t) \tag{1}$$

A time-varying model of the underwater acoustic channel (UAC) is described by Eq.(2) (Proakis, 2000), where the channel impulse response $h(t,\tau)$ now varies in time.

$$y(t) = \int_{-\infty}^{\infty} h(t,\tau)x(t-\tau)\, d\tau + n(t) \tag{2}$$

Of the many time-varying processes that alter signal propagation through an UAC, including movement of the transmitter and/or receiver, time varying sound speed profiles, and tidal changes in water depth, it is the effect of surface waves that is of experimental interest in this study.

2. TIME-VARYING CHANNEL RESPONSE ESTIMATION THEORY

The aim of channel probing (or channel sounding) is to uncover the time and delay dependencies of the real time-varying channel response $h(t,\tau)$, so that the transmission of various trial signals through the channel may be simulated by the convolution process of Eq.(2).

A channel is probed by the repeated physical transmission of a short distinctive acoustic probe signal of finite length, referred to as symbol x, and recorded as a distorted received signal y. Repeated calculation of the cross correlation of x and y then reveals successive estimates of the channel response $h(t,\tau)$.

In idealised impulse channel probing the symbol x is infinitesimally short in duration and infinitely high in amplitude with integrated area of one (i.e. a Dirac delta function δ_x), the received signal $y(t_i,\tau)$ resulting from the impulse δ_x at t_i reveals a snapshot of the channel response by Eq.(3), where $n(t)$ is the noise at the receiver.

$$y(t_i,\tau) = \int_{-\infty}^{+\infty} [h(t,\tau)\ \delta_x(t-t_i)\ ]\, d\tau\ + n(t_i+\tau) = h(t_i,\tau) + n(t_i+\tau) \tag{3}$$

For compactness in the following section the symbol '⊗' will be used to represent correlation and the asterisk symbol '∗' to represent convolution. The tilde '~' indicates analytic quantities and the raised asterisk '*' denotes the complex conjugate. If the noise is negligible in Eq.(3) the received signal $y(t_i,\tau)$ is then a copy of the channel response $h(t_{i,}\tau)$ for transmission instant t_i since the convolution of $\delta_x(t-t_i)$ with the channel response leaves the response unchanged apart from the time shift as per Eq.(4).

$$h\left(t_{i,}\tau\right) = h(t,\tau) * \delta_x(t-t_i) \tag{4}$$

For probing of shallow underwater channels where discrimination of the probe signal from noise is important (particularly the ubiquitous impulse-like noise from snapping shrimp) the probe symbol x must be of finite length and amplitude using the process of correlative channel probing (or sounding) (Molisch, 2011). The received signal $y = h\left(t_{i,}\tau\right) * x$ is then different to $h\left(t_{i,}\tau\right)$ and is also overlaid with noise. The channel response estimate $\hat{h}\left(t_{i,}\tau\right)$ resulting from the transmission commencing at instant $t_{i,}$ must then be recovered by cross-correlation of x and y.

To obtain the channel response estimate $\hat{h}\left(t_{i,}\tau\right)$, with the hat '$\widehat{\ }$' indicates an estimate, the transmit and received symbols are cross-correlated by Eq.(5). Substituting $\tilde{y} = h\left(t_{i,}\tau\right) * \tilde{x} + \tilde{n}$ into Eq.(5) gives Eq.(6), since correlation is a linearly additive process.

$$\hat{h}\left(t_{i,}\tau\right) = \tilde{x} \otimes \tilde{y} \tag{5}$$

$$\hat{h}(t_{i,}\tau) = \tilde{x} \otimes [h(t_{i,}\tau) * \tilde{x}] + \tilde{x} \otimes \tilde{n} \tag{6}$$

The correlation-to-convolution identity $\tilde{f} \otimes \tilde{g} = \tilde{f}(-t)^* * \tilde{g}(t)$ (Burdic, 1984a) is then used to rearrange Eq.(6) to Eq.(7). The associative and commutative properties of convolutions may be used to obtain Eq.(8) (Burdic, 1984b).

$$\hat{h}(t_{i,}\tau) = \tilde{x}^*(-\tau) * [h(t_{i,}\tau) * \tilde{x}(\tau)] + \tilde{x} \otimes \tilde{n} \tag{7}$$

$$\hat{h}(t_{i,}\tau) = [\tilde{x}^*(-\tau) * \tilde{x}(\tau)] * h(t_{i,}\tau) + \tilde{x} \otimes \tilde{n} \tag{8}$$

After applying the reverse correlation-to-convolution identity, the first term of Eq.(8) in square brackets is the autocorrelation of the transmit symbol x, denoted $R_{xx}(\tau)$, giving Eq.(9).

$$\hat{h}(t_{i,}\tau) = R_{xx}(\tau) * h(t_{i,}\tau) + \tilde{x} \otimes \tilde{n} \tag{9}$$

If x is chosen such that it has a very high autocorrelation at zero lag, and very low correlation at all non-zero lags, then $R_{xx}(\tau)$ behaves as a noisy band-limited approximation to the delta-function $\delta_x(t - t_i)$, and Eq.(9) bears a noisy similarity to Eq.(4). In this manner the delay resolution of the response estimate can be much shorter than the symbol duration. Importantly, the probe symbol x can be chosen such that the result of cross-correlation with the unrelated noise is low.

If the symbol x correlation with the non-signal noise is negligible, there is still noise in $\hat{h}(t_{i,}\tau)$ from non-zero $R_{xx}(\tau)$ for $\tau \neq 0$, which behave like small random Dirac delta functions. With negligible symbol-noise correlation, the decibel separation ΔN between the true response power and the noise within the estimate $\hat{h}(t_{i,}\tau)$ is determined by the ratio of the zero-lag autocorrelation peak to the maximum non-zero autocorrelation (Eq.(10)), or the “peak to off-peak ratio” (Molisch, 2011).

$$\Delta N = 20.\log\left[\frac{R_{xx}(0)}{\max\limits_{\tau \neq 0}[R_{xx}(\tau)]}\right] \tag{10}$$

The noise separation ΔN increases with longer symbol repeat period T_{probe}, but with corresponding loss of information in the real time dimension (t) due to the associated lower probe repetition rate W_{probe}.

An implicit assumption in the derivation of Eq.(9) is that $h(t_{i,}\tau) \cong h(t_i + T_{probe}, \tau)$ (Molisch, 2011). That is, the channel response has not changed appreciably over the transmission time T_{probe} of the symbol x. This assumption breaks down for long enough symbols.

By repeatedly calculating Eq.(9) at the probe repetition rate using successive recorded receiver samples $y(t_i, \tau)$, a discrete-time estimate of the time-varying channel response $h(t, \tau)$ is obtained.

3. EXTRACTING DOPPLER SHIFTS FROM THE TIME-VARYING CHANNEL RESPONSE

The Doppler on a channel transmission path may be expressed either as a path velocity shift v or as an equivalent signal Doppler frequency shift ν as linked by Eq.(11), where positive v represents a velocity that contracts the propagation path length, c is the speed of sound in water, and f_0 is the signal centre-frequency.

$$\nu / f_0 = \mathrm{v}/c \tag{11}$$

The two-dimensional spreading function, as described in van Walree et al. (2008) is a useful simultaneous representation of the arrival delay spreading and the Doppler spreading of the underwater acoustic channel response. A spreading function over the delay-Doppler plane is obtained by discrete Fourier transform of a Hilberttransformed response history, $\tilde{h}(t,\tau)$, with respect to the real-time (t) dimension as per Eq.(12). The analytic form of the response is necessary to correctly detect positive and negative frequency shifts in the response history.

$$\tilde{S}(\nu,\tau) = \mathcal{F}\left(\tilde{h}(t,\tau)\right) = \int_{-\infty}^{+\infty} \tilde{h}(t,\tau) e^{-i2\pi\nu t}\, dt \tag{12}$$

Implementing Eq.(12) as a discrete Fourier transform requires that the response history is first windowed in the time dimension to avoid spurious spectral noise from the start and end of the discrete response history estimate. This was achieved by using half a Hanning window for the first and last 10% of the history in the time direction. The total channel delay power profile $P(\tau)$ may be obtained by summation of the spreading function over all M discrete Doppler frequency shifts by Eq.(13)).

$$P(\tau) = \sum_{m=1}^{M-1} \left|\tilde{S}(\nu_m,\tau)\right|^2 \tag{13}$$

4. EXPERIMENTAL SITE, ARRANGEMENT AND CONDITIONS

Channel-probing experiments were conducted south-west of Rottnest Island near Perth as shown on Fig.1, using point-to-point transmission at ranges of 100 m to 10 km in 53m water depth. The trial was conducted with a drifting transmitter and bottom-mounted receiver within 1.5 km of a directional wave-rider buoy (DWRB) as shown on Fig.2. Photographs of the ocean surface conditions at the commencement and conclusion of testing are illustrated on Fig.3.

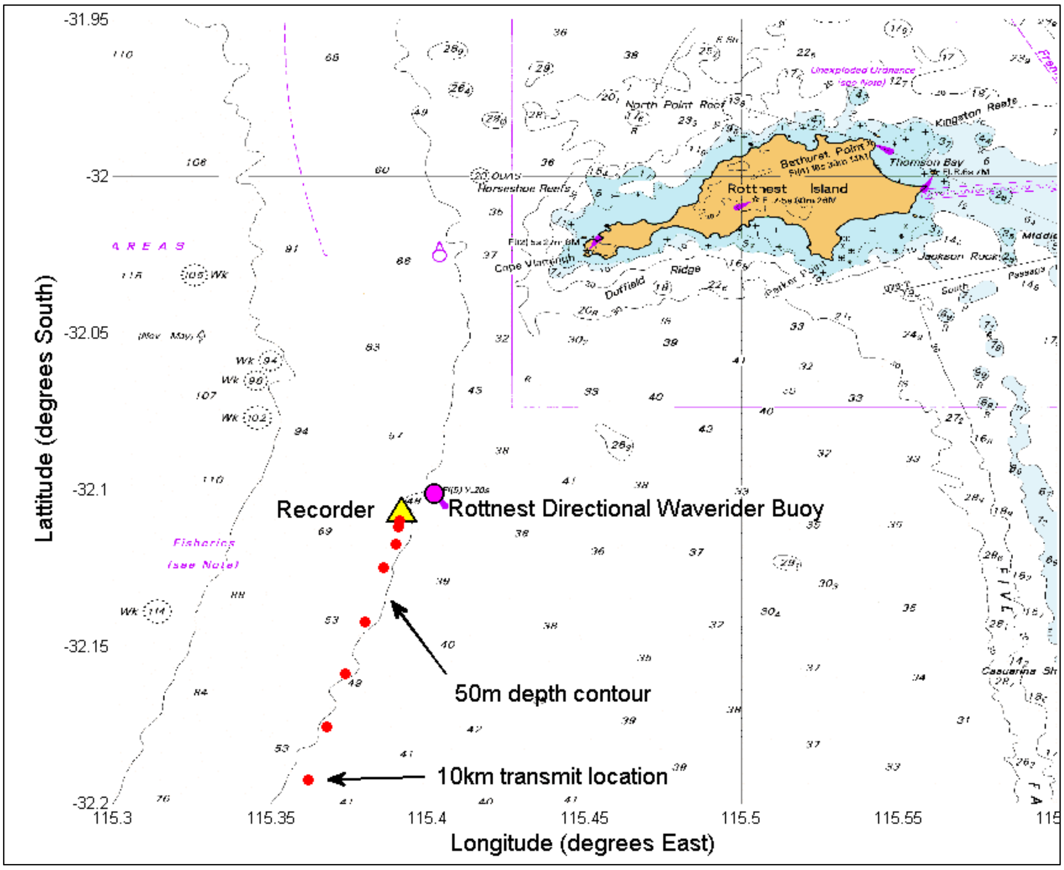

Figure 1: Transmit and record locations (base map source- Lancelin to Cape Peron 1:150 000 Aus00754)

The ocean swell and sea was generally directed from the transmitter towards the receiver, with a total significant wave height of between 1.5m and 2m, where the significant wave height is defined as four times the RMS surface wave height. Wave height and direction records from the Rottnest Island directional wave-rider buoy (DWRB) were obtained courtesy of the Western Australian Department of Transport.

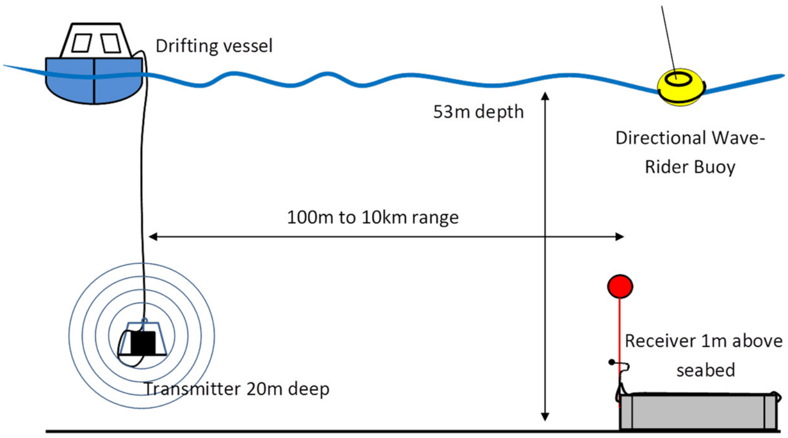

Figure 2: Schematic experimental arrangement

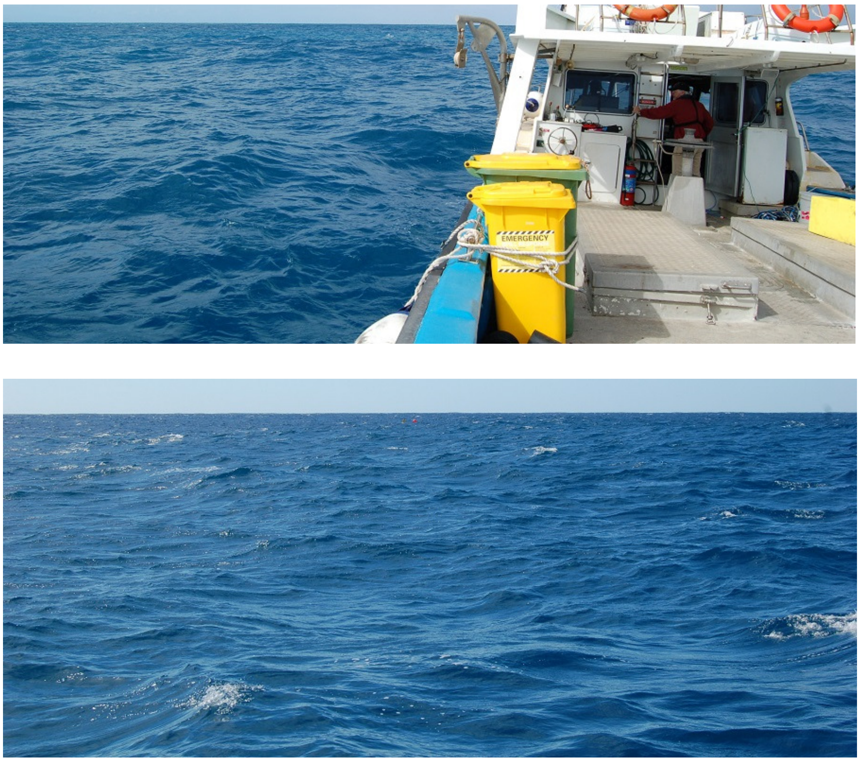

Figure 3: Experimental sea surfaces - morning (top), and at end of last transmission at 3 pm (bottom)

The sound speed profile at a number of transmission positions was sampled with a Seabird SBE 19Plus Conductivity Temperature Depth (CTD) probe. The profiles, such as the sample at the southern-most end of the range plotted on Fig.4, indicated warming of the surface waters over the period of the experiment to the extent of approximately 0.5 m/s sound speed differential.

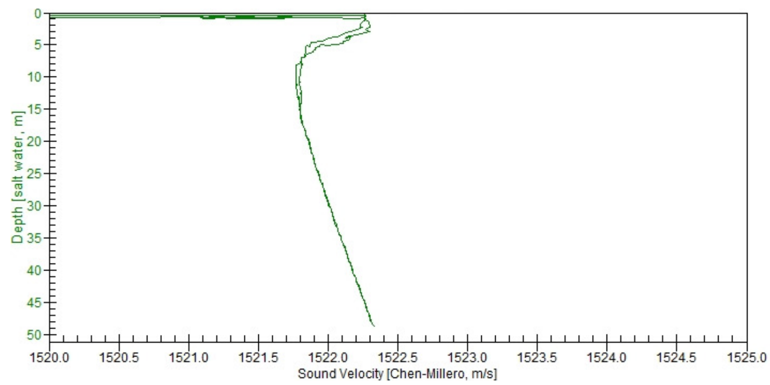

Figure 4: Sound speed profile CTD Cast 6 –12:40 pm – 10 km SSW of receiver

5. SELECTION OF PROBE SIGNALS

Determining the likely delay spread of measurable multi-path signal arrivals in advance of a field trial is uncertain, as it depends on the strength of successive multiple surface-reflected propagation paths. A flatter sea-surface will enable paths with a higher number of surface-bottom reflections (and longer associated delay) to be detectable at the receiver, and vice versa.

The Bellhop model (Porter, 2011) was run at a number of ranges to check the delay spread in 50m water depth prior to field testing. In the event that the signal was too degraded after two surface bounces to enable detection, it was reasoned that the probe signal should at least be longer than the single-bounce-path delays to enable exploration of the single-surface-interacting channel delay structure.

Guided by this consideration, the shortest probe symbol, a 63 element spread-spectrum Pseudo-Random Binary Sequence design (PRBS), was chosen having 21 ms length. This would enable the channel response to be updated at a rate of 1/21 ms = 47.6 Hz. A binary switching frequency of 3 kHz, commonly referred to as the 'chipping' frequency, was used to achieve a 6 kHz bandwidth. The sinusoidal carrier centre-frequency was chosen at 12 kHz to enable the bandwidth to fall within the relatively even power plateau in the CTG0052 transducer transmit characteristic. The signal power outside of the desired nominal 9 kHz to 15 kHz band-width was minimised by sinc-shaping the bi-polar modulated sequence (Schanze, 1995), as shown in the middle graph on Figure 5 for the shortest 21 ms PRBS. A much longer 4095 element PRBS symbol of 1.4 s duration was included to enable time-domain Doppler search.

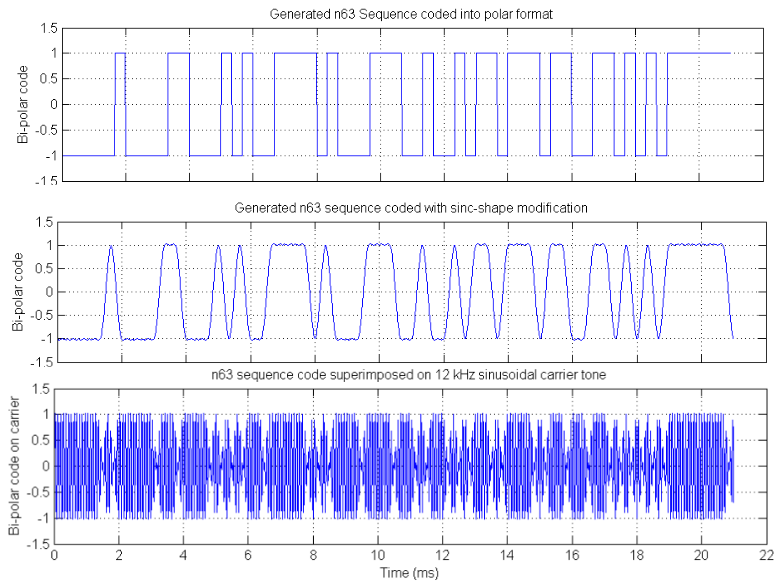

Figure 5: Example generation of 21 ms PRBS probe signal

As the optimal length probe symbol cannot be established apriori a composite test signal is synthesised of probe symbols of different lengths and repeat intervals, with correlation analysis conducted on the symbol(s) that best matches the experimental channel delay and Doppler spread.

The goal of the probe signal design was to achieve a 21 ms channel update rate in an environment with an anticipated arrival delay spread of up to 150 ms, depending on range. In an attempt to achieve this whilst maintaining a channel sampling rate of 48 Hz, a set of 8 x 21 ms orthogonal pseudo random binary sequence (PRBS) probes was constructed (Gold Code set (Proakis, 2000)), having the high autocorrelation property of PRBS sequences, and as low as possible cross-correlation property within the set. A combination of the small dynamic range available for the relatively short 21 ms Gold code set and problems with their implementation meant that useful channel responses were measured using proven 21 ms PRBS, 1.4 s PRBS and 16 ms 8-16 kHz LFM sweep probe symbols. The LFM sweep repeat interval was altered with range to maximise the channel sampling rate. The trial also included coded data sequences provided by Prof. Yue Rong's communications research group within the Curtin Dept. Electrical and Computer Engineering.

Table 1 summarises the probe symbols used and Table 2 summarises the anticipated channel delay-spread with range, and the series of sequences used to measure the channel responses. Each full transmit signal totalled 668s.

Table 1: Rottnest trial probe symbols

Signal descriptor	Carrier frequency f_o (kHz)	Symbol repeat period T (s)	Bandwidth B (kHz)
n4095 PRBS	12	1.365	6
n63 PRBS Gold code set	12	0.021	6
n63PRBS	12	0.021	6
16 ms LFM sweep	8-16	50 ms to 200 ms	8

Table 2: Probe signal composition versus transmission range

<table>
<tr><th>Range</th><th>Estimated delay spread</th><th>21 ms PRBS</th><th>1.36 s PRBS</th><th>16 ms 8 kHz-16 kHz linear sweep</th><th>21 ms M6 Gold code cycle</th><th>Computer Eng. Signal</th></tr>
<tr><td>125 m</td><td>150 ms</td><td rowspan="9">60 s of repeats</td><td rowspan="9">60 s of repeats</td><td rowspan="3">60 s at 200 ms repeat interval</td><td rowspan="3">60 s of 8x21 ms cycle</td><td rowspan="6">4 minutes qpsk + 3 minutes 8psk</td></tr>
<tr><td>250 m</td><td>106 ms</td></tr>
<tr><td>500 m</td><td>104 ms</td></tr>
<tr><td>1 km</td><td>58 ms</td><td rowspan="2">60 s at 100 ms repeat interval</td><td rowspan="2">60 s of 4x21 ms cycle</td></tr>
<tr><td>2 km</td><td>45 ms</td></tr>
<tr><td>4 km</td><td>23 ms</td><td rowspan="4">60 s at 50 ms repeat interval</td><td rowspan="4">60 s of 2x21 ms cycle</td></tr>
<tr><td>6 km</td><td>21 ms</td><td rowspan="2">4 minutes bpsk + 3 minutes qpsk</td></tr>
<tr><td>8 km</td><td>16 ms</td></tr>
<tr><td>10 km</td><td>13 ms</td><td>7 minutes bpsk</td></tr>
</table>

6. RESULTS

6.1 Time-varying channel responses

Three example measured time-varying channel response estimates of 60 seconds duration are presented in Figure 6 for 121m, 1102m and 7827m ranges. Each plot was created from successive channel response estimates in the (vertical) time dimension, using a 16ms 8-16 kHz sweep. At 121m range (top plot) the long sweep repeat interval of 150ms enables detection of the fainter responses from double surface interacting paths. The relatively straight vertical response represents the combined response of the direct and bottom-bounce paths which do not interact with the sea surface. The broad response at around 10ms represents transmission paths that have interacted just once with the ocean surface.

At 1102m range (lower left plot) the shallow angle of surface interacting paths enables the response from paths with three successive surface interactions to be clearly captured. At 7827m further reduction in grazing angle enables detection of responses from paths with as many as five surface interactions.

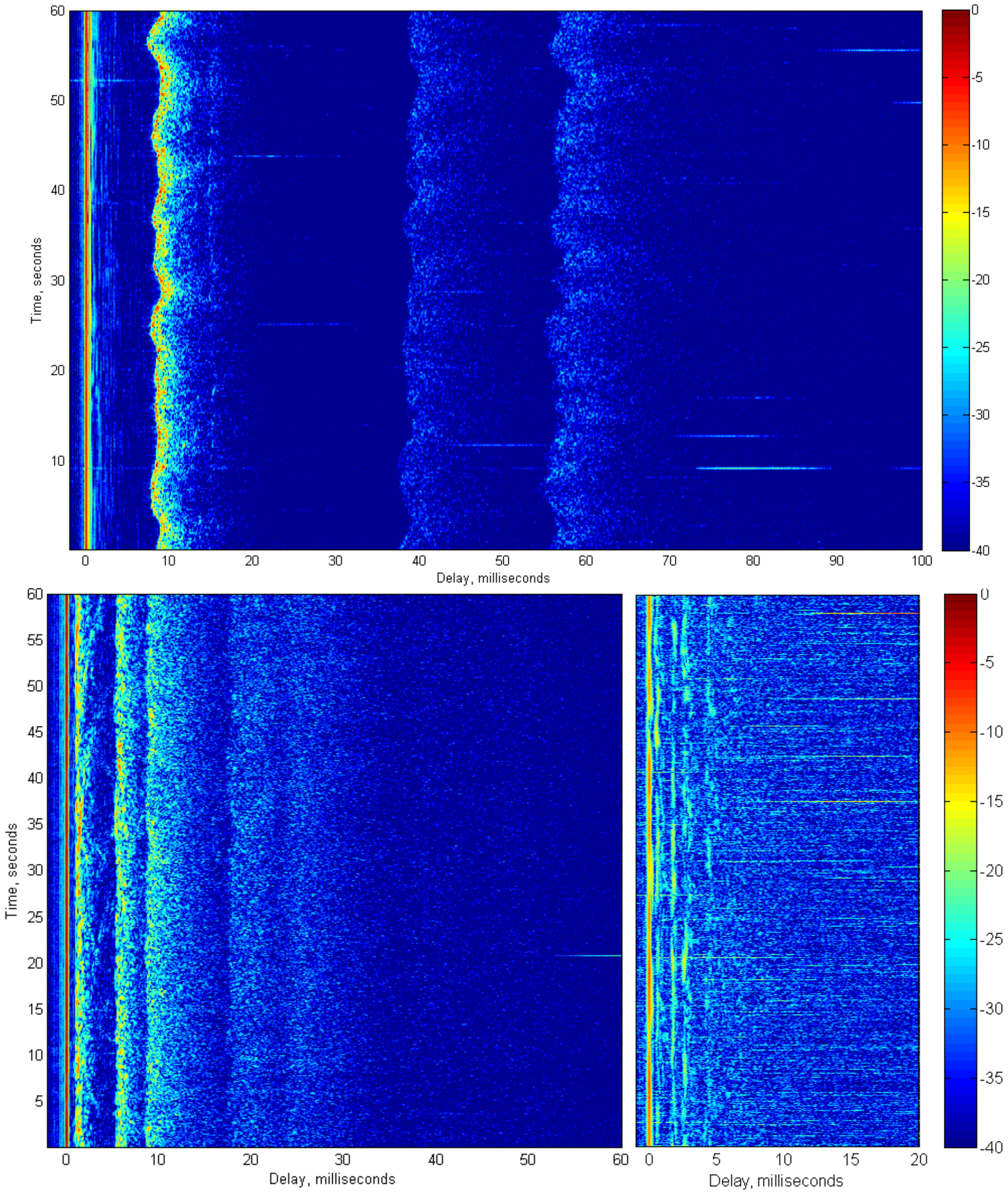

Figure 6: Measured channel response, $20\log\left|\hat{h}(t,\tau)\right|$, (dB) using 16 ms 8 -16 kHz LFM sweep at ranges of 121 m (top), 1102 m (lower left), and 7827 m (lower right)

6.2 Power-delay profiles

The average power delay profiles corresponding to the time-varying responses in Figure 6 are presented in Figure 7. These profiles have been normalised relative to the response of the first path arrival, which is normally the direct path response at short range (e.g. 121m), and a coalescence of single surface-bounce paths at longer range (e.g.7827m). At intermediate ranges the presence or absence of a direct-path response is dependent on the sound speed profile, which determines whether or not a direct sound path exists between the source and receiver.

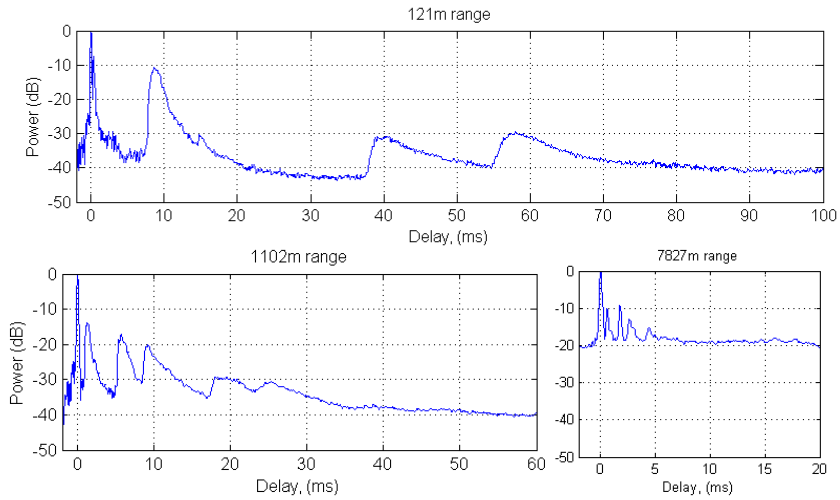

Figure 7: Measured response power versus delay, $10\log\left|\hat{P}(\tau)\right|$ (dB) using 16 ms 8 -16 kHz LFM sweep at ranges of 121 m (top), 1102 m (lower left), and 7827 m (lower right)

6.3 Channel spreading functions

The experimental channel spreading functions obtained from the time-varying channel responses using Eq.(12) are presented in Figure 8. These plots were necessarily obtained from the time-varying response obtained for the 21ms probe at slightly different ranges to the responses in Figure 6. The 48 Hz repeat frequency of this probe is necessary to capture the short-range Doppler on the steepest single-surface bounce responses at 137m. Whilst the sweep at 150ms repeat interval is able to capture greater delay spreading detail (top of Figure 6), the lower repeat frequency of just 6.6 Hz means that the Doppler frequency window on the spreading function is just 6.6 Hz, insufficient to capture short range Doppler spreading.

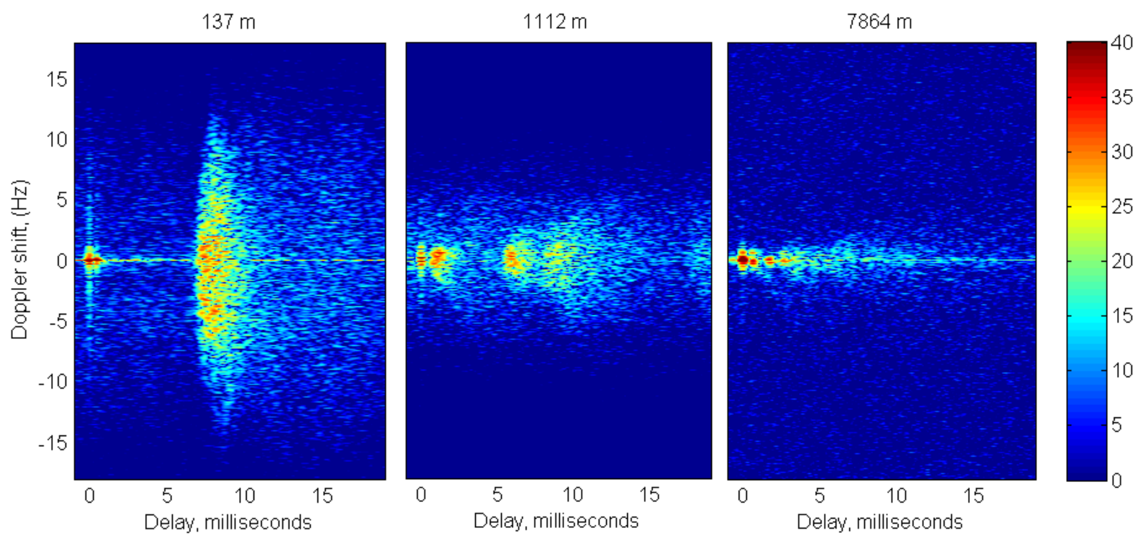

Figure 8: Measured spreading function from 21ms PRBS probe, $20\log\left|\hat{S}(\nu,\tau)\right|$ (dB),$f_0 12$ kHz, 137 m range (left), 1112 m range (centre), and 7864 m range (right)

7. Discussion

Figure 8 illustrates that the Doppler distortion of the signal received via surface interacting paths increases as the range decreases. This presents interesting challenges for the design of communication receiver signal processing algorithms.

Counter-intuitively it can be at medium ranges when extraction of data from a communication is most problematic. At short range the significant delay between the direct path and subsequent arrivals via surface-interacting paths enables robust algorithms to be built into communication receivers to target the relatively undistorted first-arriving signal that has travelled via direct and bottom paths.

At long range the wave-guide behavior sees the convergence of near-horizontal diverse transmission path lengths and reduced influence of surface-waves on path length variations (and therefore Doppler) produce a stable coherent signal from surface-interacting paths with minimal Doppler distortion.

At intermediate ranges three factors can combine to make demodulation of the signal more difficult than at both shorter and longer ranges. The first-arriving signal may or may not be distorted by surface interaction. If there is a non-surface interacting first arrival it may be very closely spaced in delay to the first arrivals from surface interacting paths. If there is no non-surface interacting path the Doppler shifting on the first arrival may be significant and unpredictable.

It is worth noting that the above analysis presents the channel response at three ranges for just one surface condition, one transmit direction relative to the prevailing directional ocean waves, one combination of transmitter and receiver depth and one sound speed profile. There are also subtle differences in channel response that depend on the probe symbol used. Changing any one of these circumstances will produce a different time-varying channel response, underscoring the value and original motivation for development of a UAC simulator.

8. ACKNOWLEDGEMENTS

The assistance of Dr Tim Gourlay and Prof. Yue Rong at sea was greatly appreciated by the authors during this experimental trial. The assistance of Mr Frank Thomas and Mr Mal Perry with preparation of acoustic instrumentation and moorings was also appreciated. This project was supported under the Australian Research Council's Discovery Projects funding scheme (project number DP110100736) and by L3-Communications Oceania Ltd.

9. REFERENCES

Burdic, W. S. 1984a. Correlation and Correlation Functions. *Underwater Acoustic System Analysis.* Englewood Cliffs, NJ: Prentice-Hall.

Burdic, W. S. 1984b. Fourier Methods. *Underwater Acoustic System Analysis.* Englewood Cliffs, NJ: Prentice-Hall.

Caley, M. S. 2016. Development of a dynamic underwater acoustic communication channel simulator with configurable sea surface parameters to explore time-varying signal distortion. Ph.D Dissertation, Curtin University of Technology. Available: http://link.library.curtin.edu.au/p?cur_digitool_dc241262.

Caley, M. S. & Duncan, A. J. 2013. Investigation of underwater acoustic multi-path Doppler and delay spreading in a shallow marine environment. *Acoustics Australia,* 41**,** 20-28.

Eggen, T. H., Baggeroer, A. B. & Preisig, J. C. 2000. Communication over Doppler spread channels - Part I: Channel and receiver presentation. *IEEE Journal of Oceanic Engineering,* 25**,** 62-71.

Molisch, A. 2011. Channel Sounding. *Wireless Communications.* Wiley-IEEE Press.

Porter, M. B. 2011. The BELLHOP Manual and Users Guide - *preliminary draft*. Available: http://oalib.hlsresearch.com/Rays/HLS-2010-1.pdf.

Proakis, J. G. 2000. *Digital Communications,* New York, McGraw Hill.

Schanze, T. 1995. Sinc interpolation of discrete periodic signals. *IEEE Transactions on Signal Processing,* 43**,** 1502-1503.

van Walree, P. A., Jenserud, T. & Smedsrud, M. 2008. A Discrete-Time Channel Simulator Driven by Measured Scattering Functions. *IEEE Journal on Selected Areas in Communications,* 26**,** 1628-1637.